The Jupiter Laser Facility - HED Science

Robert Cauble

JLF Director

West Coast HED Cooperative Workshop

This work was performed under the auspices of the U.S. Department of Energy by Lawrence Livermore National Security, LLC, Lawrence Livermore National Laboratory under Contract DE-AC52-07NA27344.

LLNL-PRES-614335

Jupiter/Janus (5th-highest-energy research laser in US)

Long-pulse Janus is used mainly for HED matter and materials studies: EOS (VISAR), *in situ* dynamics (diffraction), HED chemistry (CARS)

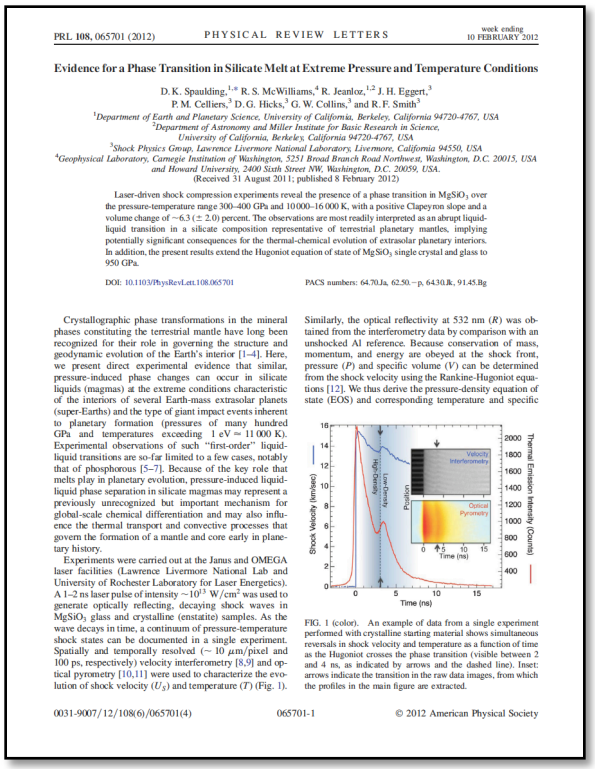

PRL 108, 065701 (2012) PHYSICAL REVIEW LETTERS week ending 10 FEBRUARY 2012

Evidence for a Phase Transition in Silicate Melt at Extreme Pressure and Temperature Conditions

D. K. Spaulding,[1,*] R. S. McWilliams,[4] R. Jeanloz,[1,2] J. H. Eggert,[3] P. M. Celliers,[3] D. G. Hicks,[3] G. W. Collins,[3] and R. F. Smith[3]

[1]*Department of Earth and Planetary Science, University of California, Berkeley, California 94720-4767, USA*
[2]*Department of Astronomy and Miller Institute for Basic Research in Science, University of California, Berkeley, California 94720-4767, USA*
[3]*Shock Physics Group, Lawrence Livermore National Laboratory, Livermore, California 94550, USA*
[4]*Geophysical Laboratory, Carnegie Institution of Washington, 5251 Broad Branch Road Northwest, Washington, D.C. 20015, USA and Howard University, 2400 Sixth Street NW, Washington, D.C. 20059, USA.*
(Received 31 August 2011; published 8 February 2012)

Laser-driven shock compression experiments reveal the presence of a phase transition in $MgSiO_3$ over the pressure-temperature range 300–400 GPa and 10 000–16 000 K, with a positive Clapeyron slope and a volume change of $\sim 6.3 (\pm 2.0)$ percent. The observations are most readily interpreted as an abrupt liquid-liquid transition in a silicate composition representative of terrestrial planetary mantles, implying potentially significant consequences for the thermal-chemical evolution of extrasolar planetary interiors. In addition, the present results extend the Hugoniot equation of state of $MgSiO_3$ single crystal and glass to 950 GPa.

DOI: 10.1103/PhysRevLett.108.065701 PACS numbers: 64.70.Ja, 62.50.−p, 64.30.Jk, 91.45.Bg

Crystallographic phase transformations in the mineral phases constituting the terrestrial mantle have long been recognized for their role in governing the structure and geodynamic evolution of the Earth's interior [1–4]. Here, we present direct experimental evidence that similar, pressure-induced phase changes can occur in silicate liquids (magmas) at the extreme conditions characteristic of the interiors of several Earth-mass extrasolar planets (super-Earths) and the type of giant impact events inherent to planetary formation (pressures of many hundred GPa and temperatures exceeding 1 eV ≈ 11 000 K). Experimental observations of such "first-order" liquid-liquid transitions are so-far limited to a few cases, notably that of phosphorous [5–7]. Because of the key role that melts play in planetary evolution, pressure-induced liquid-liquid phase separation in silicate magmas may represent a previously unrecognized but important mechanism for global-scale chemical differentiation and may also influence the thermal transport and convective processes that govern the formation of a mantle and core early in planetary history.

Experiments were carried out at the Janus and OMEGA laser facilities (Lawrence Livermore National Lab and University of Rochester Laboratory for Laser Energetics). A 1–2 ns laser pulse of intensity $\sim 10^{13}$ W/cm^2 was used to generate optically reflecting, decaying shock waves in $MgSiO_3$ glass and crystalline (enstatite) samples. As the wave decays in time, a continuum of pressure-temperature shock states can be documented in a single experiment. Spatially and temporally resolved (~ 10 μm/pixel and 100 ps, respectively) velocity interferometry [8,9] and optical pyrometry [10,11] were used to characterize the evolution of shock velocity (U_S) and temperature (T) (Fig. 1).

Similarly, the optical reflectivity at 532 nm (R) was obtained from the interferometry data by comparison with an unshocked Al reference. Because conservation of mass, momentum, and energy are obeyed at the shock front, pressure (P) and specific volume (V) can be determined from the shock velocity using the Rankine-Hugoniot equations [12]. We thus derive the pressure-density equation of state (EOS) and corresponding temperature and specific

FIG. 1 (color). An example of data from a single experiment performed with crystalline starting material shows simultaneous reversals in shock velocity and temperature as a function of time as the Hugoniot crosses the phase transition (visible between 2 and 4 ns, as indicated by arrows and the dashed line). Inset: arrows indicate the transition in the raw data images, from which the profiles in the main figure are extracted.

Shock vaporization of silica and the thermodynamics of planetary impact events

R. G. Kraus,[1] S. T. Stewart,[1] D. C. Swift,[2] C. A. Bolme,[3] R. F. Smith,[2] S. Hamel,[2] B. D. Hammel,[2] D. K. Spaulding,[4] D. G. Hicks,[2] J. H. Eggert,[2] and G. W. Collins[2]

Received 15 March 2012; revised 17 August 2012; accepted 18 August 2012; published 28 September 2012.

[1] The most energetic planetary collisions attain shock pressures that result in abundant melting and vaporization. Accurate predictions of the extent of melting and vaporization require knowledge of vast regions of the phase diagrams of the constituent materials. To reach the liquid-vapor phase boundary of silica, we conducted uniaxial shock-and-release experiments, where quartz was shocked to a state sufficient to initiate vaporization upon isentropic decompression (hundreds of GPa). The apparent temperature of the decompressing fluid was measured with a streaked optical pyrometer, and the bulk density was inferred by stagnation onto a standard window. To interpret the observed post-shock temperatures, we developed a model for the apparent temperature of a material isentropically decompressing through the liquid-vapor coexistence region. Using published thermodynamic data, we revised the liquid-vapor boundary for silica and calculated the entropy on the quartz Hugoniot. The silica post-shock temperature measurements, up to entropies beyond the critical point, are in excellent qualitative agreement with the predictions from the decompressing two-phase mixture model. Shock-and-release experiments provide an accurate measurement of the temperature on the phase boundary for entropies below the critical point, with increasing uncertainties near and above the critical point entropy. Our new criteria for shock-induced vaporization of quartz are much lower than previous estimates, primarily because of the revised entropy on the Hugoniot. As the thermodynamics of other silicates are expected to be similar to quartz, vaporization is a significant process during high-velocity planetary collisions.

Citation: Kraus, R. G., et al. (2012), Shock vaporization of silica and the thermodynamics of planetary impact events, *J. Geophys. Res.*, *117*, E09009, doi:10.1029/2012JE004082.

1. Introduction

[2] During the end stage of planet formation, the nebular gas disperses and mutual encounter velocities increase via gravitational stirring from the largest bodies. *N*-body simulations of this stage find typical collision velocities between protoplanets of one to a few times the two-body escape velocity [*Agnor et al.*, 1999]. The kinetic energy of an impact is partially transferred to internal energy in the colliding bodies via passage of a strong shock wave. At the expected impact velocities of ~10 to a few tens of km s^{-1} sufficient to melt and vaporize a large fraction of the colliding bodies. However, the predicted degree of melting and vaporization for a specific impact scenario has great uncertainty that primarily arises from poorly-constrained equations of state (EOS).

[3] Accurate equations of state over a tremendous region of phase space are required to make predictions about the impact processes so prevalent during the formation of the solar system and its subsequent evolution. The last giant impact is invoked to explain the diverse characteristics of rocky and icy planets in the Solar System [e.g., *Stewart and Leinhardt*, 2012], including the large core of Mercury [*Benz et al.*, 1988, 2007], formation of Earth's moon [*Canup and Asphaug*, 2001], Pluto's moons [*Canup*, 2005], and Haumea's moons and family members [*Leinhardt et al.*, 2010]. In each case, the argument for a giant impact relies upon the details of the equations of state.

[4] Although equation of state theory is advancing rapidly, the generation of accurate and complete equations of state from first principles is still not feasible for most geologic materials. Planetary collisions are particularly challenging because of the need to understand both the extreme temperatures and high compression ratios achieved in the

[1]Department of Earth and Planetary Sciences, Harvard University, Cambridge, Massachusetts, USA.
[2]Lawrence Livermore National Laboratory, Livermore, California, USA.
[3]Los Alamos National Laboratory, Los Alamos, New Mexico, USA.
[4]Department of Earth and Planetary Sciences, University of California, Berkeley, California, USA.

Corresponding author: R. G. Kraus, Department of Earth and Planetary Sciences, Harvard University, 20 Oxford St., Cambridge, MA 02138, USA. (rkraus@fas.harvard.edu)

0148-0227/12/2012JE004082

(Fig. 3A). Pt deposition resulted in three distinct levels of contrast that reflect the surface height, with the lowest level being the original Au terraces (Fig. 3B). The same three-level structure was observed independently of deposition time up to 500 s (Fig. 3C). The middle contrast level corresponds to a high density of Pt islands that covered ~85% of the Au surface, with a step height of ~0.24 nm, consistent with XPS results. Inspection with a higher rendering contrast revealed a ~10% coverage of a second layer of small Pt islands with a step height ranging between 0.23 and 0.26 nm (Fig. 3D). Step positions associated with the flame-annealed substrate were preserved, with negligible expansion or overgrowth of the 2D Pt islands occurring beyond the original step edge. The lateral span of the Pt islands was 2.02 ± 0.38 nm, corresponding to an area of 4.23 ± 1.97 nm^2. Incipient coalescence of the islands was constrained by surrounding (dark) narrow channels, 2.1 ± 0.25 nm wide, that account for the remaining Pt-free portion of the first layer. The reentrant channels correspond to open Au terrace sites that were surrounded by adjacent Pt islands in what amounted to a huge increase in step density relative to the original substrate, the net geometric or electronic effect of which was to block further Pt deposition. The chemical nature of the inter-island region was assayed by exploiting the distinctive voltammetry of Pt and Au with respect to H_{ad} and oxide formation and reduction (fig. S2 and supplementary text).

Similar three-level Pt overlayers have been observed for monolayer films produced by molecular beam epitaxy (MBE) deposition at 0.05 monolayers/min (*20*). Pt-Au intermixing driven by the decrease in surface energy that accompanies Au surface segregation was evident. In the present work, Pt monolayer formation was effectively complete within 1 s, giving a growth rate three orders of magnitude greater than in the MBE-STM study. Exchange of the deposited Pt with the underlying Au substrate was expected to be less developed. However, intermixing and possible chemical contrast (i.e., the ligand effect) were evident on limited sections of the surface that were correlated with the original faulted geometry of the partially reconstructed Au surface. Upon lifting of the reconstruction, the excess Au atoms expelled mark the original fault location as linear 1D surface defects in the Pt overlayer (Fig. 3E). A simplified schematic of the self-terminating Pt deposition process in Fig. 3F describes how the H_{ad} accompanying incremental expansion of the 2D Pt islands can hinder the development of a second Pt layer, presumably by perturbation of the overlying water structure (*17*). This rapid process resulted in a much higher Pt island coverage than has been obtained by other methods, such as galvanic exchange reactions.

Because the saturated H_{ad} coverage is the agent of termination, reactivation for further Pt deposition was possible by removing the upd layer by sweeping or stepping the potential to positive values, e.g., >+0.2 V_{SCE}, where negligible Pt deposition occurs. Sequential pulsing between +0.4 V_{SCE} and −0.8 V_{SCE} enabled Pt monolayer deposition to be controlled in a digital manner. EQCM was used to track the mass gain, showing two net increments per cycle (Fig. 4A). We attributed the mass gain to a combination of Pt deposition [486 ng/cm^2 for a monolayer of Pt(111)], anion adsorption and desorption (41 ng/cm^2 for 7 × 10^{14} Cl$^-$ ion/cm^2, 117 ng/cm^2 for a 0.14 fractional coverage of $PtCl_4^{2-}$) (*7*, *21*), and coupling to other double-layer components such as water. The anionic mass increments were expected to be asymmetric for the first cycle on the Au surface, but once it was covered, subsequent cycles only involved Pt surface chemistry. After correcting for the electroactive surface area of the Au electrode ($A_{real}/A_{geometric}$ = 1.2, derived from reductive desorption of Au oxide in perchloric acid), the net mass gain for each cycle indicates that a near-pseudomorphic layer of Pt was deposited. XPS analysis of Pt films grown in various deposition cycles give remarkably good agreement with EQCM data (Fig. 4B). The ability to rapidly manipulate potential and double-layer structure, as opposed to the exchange of reactants, offers simplicity, substantially improved process efficiency, and far greater process speed than other surface-limited deposition methods.

References and Notes

1. F. T. Wagner, R. Lakshmanan, M. F. Mathias, *J. Phys. Chem. Lett.* **1**, 2204 (2010).
2. M. K. Debe, *Nature* **486**, 43 (2012).
3. M. T. M. Koper, Ed., *Fuel Cell Catalysis, A Surface Science Approach* (Wiley, Hoboken, NJ, 2009).
4. V. R. Stamenkovic *et al.*, *Nat. Mater.* **6**, 241 (2007).
5. R. R. Adzic *et al.*, *Top. Catal.* **46**, 249 (2007).
6. T. Michely, J. Krug, *Islands, Mounds and Atoms, Patterns and Processes in Crystal Growth Far from Equilibrium* (Springer Series in Surface Science, V42, Springer, New York, 2003).
7. H. F. Waibel, M. Kleinert, L. A. Kibler, D. M. Kolb, *Electrochim. Acta* **47**, 1461 (2002).
8. T. Kondo *et al.*, *Electrochim. Acta* **55**, 8302 (2010).
9. I. Bakos, S. Szabo, T. Pajkossy, *J. Solid State Electrochem.* **15**, 2453 (2011).
10. S. R. Brankovic, J. X. Wang, R. R. Adzic, *Surf. Sci.* **474**, L173 (2001).
11. D. Golcen, S.-E. Bae, S. R. Brankovic, *Electrochim. Acta* **56**, 5545 (2011).
12. B. W. Gregory, J. L. Stickney, *J. Electroanal. Chem.* **300**, 543 (1991).
13. A. J. Gregory, W. Levason, R. E. Noftle, R. Le Penven, D. Pletcher, *J. Electroanal. Chem.* **399**, 105 (1995).
14. See supplementary materials on *Science* Online.
15. N. Garcia-Araez, V. Climent, E. Herrero, J. Feliu, J. Lipkowski, *J. Electroanal. Chem.* **582**, 76 (2005).
16. D. Strmcnik, D. Tripkovic, D. van der Vliet, V. Stamenkovic, N. M. Markovic, *Electrochem. Commun.* **10**, 1602 (2008).
17. T. Roman, A. Groß, Structure of water layers on hydrogen-covered Pt electrodes, *Catalysis Today*; http://dx.doi.org/10.1016/j.cattod.2012.06.001 (2012).
18. G. Jerkiewicz, G. Vatankhah, S. Tanaka, J. Lessard, *Langmuir* **27**, 4220 (2011).
19. P. J. Cumpson, M. P. Seah, *Surf. Interface Anal.* **25**, 430 (1997).
20. M. O. Pedersen *et al.*, *Surf. Sci.* **426**, 395 (1999).
21. Y. Nagahara *et al.*, *J. Phys. Chem. B* **108**, 3224 (2004).

Acknowledgments: We thank J. J. Mallett for his early observations on the difficulty of electrodepositing Pt films at negative potentials. This work was supported by NIST–National Measurement Laboratory programs. The x-ray photoelectron spectrometer was provided by NIST–American Recovery and Reinvestment Act funds. Y.L. thanks the NIST–National Research Council Postdoctoral Fellowship Program for support. NIST has filed a provisional patent application (Atomic Layer Deposition of Pt from Aqueous Solutions) based on this work.

Supplementary Materials

www.sciencemag.org/cgi/content/full/338/6112/1327/DC1
Materials and Methods
Supplementary Text
Figs. S1 and S2
References (*22*–*26*)

16 August 2012; accepted 17 October 2012
10.1126/science.1228925

Phase Transformations and Metallization of Magnesium Oxide at High Pressure and Temperature

R. Stewart McWilliams,[1,2]*† Dylan K. Spaulding,[3]‡ Jon H. Eggert,[4] Peter M. Celliers,[4] Damien G. Hicks,[4] Raymond F. Smith,[4] Gilbert W. Collins,[4] Raymond Jeanloz[3,5]

Magnesium oxide (MgO) is representative of the rocky materials comprising the mantles of terrestrial planets, such that its properties at high temperatures and pressures reflect the nature of planetary interiors. Shock-compression experiments on MgO to pressures of 1.4 terapascals (TPa) reveal a sequence of two phase transformations: from B1 (sodium chloride) to B2 (cesium chloride) crystal structures above 0.36 TPa, and from electrically insulating solid to metallic liquid above 0.60 TPa. The transitions exhibit large latent heats that are likely to affect the structure and evolution of super-Earths. Together with data on other oxide liquids, we conclude that magmas deep inside terrestrial planets can be electrically conductive, enabling magnetic field–producing dynamo action within oxide-rich regions and blurring the distinction between planetary mantles and cores.

Magnesium oxide (MgO) is among the simplest oxides constituting the rocky mantles of terrestrial planets such as Earth and the cores of Jupiter and other giant planets. Present in Earth's mantle as an end-member component of the mineral $(Mg,Fe)O$ magnesiowüstite,

Physical and Life SCIENCES

Jupiter/Titan

High-energy ps Titan is used for HED plasma experiments: Technique development and implementation (XRTS); FI (particle transport); WDM (x-ray, VISAR, and particle diagnostics), relativistic plasmas (transport, LPI)

PRL 108, 115004 (2012) PHYSICAL REVIEW LETTERS week ending 16 MARCH 2012

Hot Electron Temperature and Coupling Efficiency Scaling with Prepulse for Cone-Guided Fast Ignition

T. Ma,[1,2] H. Sawada,[2] P. K. Patel,[1] C. D. Chen,[1] L. Divol,[1] D. P. Higginson,[1,2] A. J. Kemp,[1] M. H. Key,[1] D. J. Larson,[1] S. Le Pape,[1] A. Link,[1,3] A. G. MacPhee,[1] H. S. McLean,[1] Y. Ping,[1] R. B. Stephens,[4] S. C. Wilks,[1] and F. N. Beg[2]

[1]*Lawrence Livermore National Laboratory, Livermore, California 94550, USA*
[2]*University of California-San Diego, La Jolla, California 92093, USA*
[3]*The Ohio State University, Columbus, Ohio 43210, USA*
[4]*General Atomics, San Diego, California 92186, USA*
(Received 3 December 2011; published 16 March 2012)

The effect of increasing prepulse energy levels on the energy spectrum and coupling into forward-going electrons is evaluated in a cone-guided fast-ignition relevant geometry using cone-wire targets irradiated with a high intensity (10^{20} W/cm^2) laser pulse. Hot electron temperature and flux are inferred from $K\alpha$ images and yields using hybrid particle-in-cell simulations. A two-temperature distribution of hot electrons was required to fit the full profile, with the ratio of energy in a higher energy (MeV) component increasing with a larger prepulse. As prepulse energies were increased from 8 mJ to 1 J, overall coupling from laser to all hot electrons entering the wire was found to fall from 8.4% to 2.5% while coupling into only the 1–3 MeV electrons dropped from 0.57% to 0.03%.

DOI: 10.1103/PhysRevLett.108.115004 PACS numbers: 52.50.Jm, 52.38.Kd, 52.38.Mf, 52.70.La

Fast Ignition (FI) [1,2] is an approach to inertial confinement fusion (ICF), in which a precompressed deuterium-tritium fuel is rapidly driven to ignition by an external heat source. This scheme can ignite lower density fuel leading, in principle, to higher gains than possible with conventional ignition. In the reentrant cone approach to FI, a hollow cone is embedded in the fuel capsule to provide an open evacuated path free of coronal plasma for an intense laser beam to generate a flux of energetic electrons at the tip of the cone which can then propagate to the compressed fuel core. However, the presence of preformed plasma in the cone, arising from the inherent laser prepulse which ablates the inner cone wall, can strongly affect the spatial, energy-spectral, and angular characteristics of these laser-generated hot electrons and thus the efficiency with which their energy can be coupled to the core.

Previous works by Baton *et al.* [3] and Van Woerkom *et al.* [4] showed that significant prepulse could have a detrimental effect on coupling beyond the cone tip. MacPhee *et al.* [5] demonstrated that even a small prepulse could result in significant filamentation of the laser beam in the preplasma, limiting the penetration of the laser, and accelerating energetic electrons transversely. These results were achieved using either imaging of $K\alpha$ x-ray emission from the cone target itself or measuring the intensity of the $K\alpha$ spot in a region beyond the cone tip. However, while these techniques provided a spatial distribution of $K\alpha$ in various areas of the interaction, no spectral information regarding the electron flux could be inferred. Comparisons of preplasma versus no preplasma conditions by Baton *et al.* were achieved by doubling the fundamental laser frequency to create a high contrast. This provided a clean interaction surface for the main laser, but complicated the comparison, as the absorption mechanisms would be different for the very different $I\lambda^2$. In the MacPhee *et al.* study, electrons were electrostatically confined within the isolated cone target. The significant amount of recirculation of the hot electrons within the cone walls and plasma allows only limited conclusion of the electron source at the cone tip in either the experiment or simulations.

In this Letter, we present the first quantitative scaling of coupling as a function of prepulse in an intense laser-cone interaction. Through the use of cone-wire targets [6], we demonstrate the existence of a two-temperature hot electron distribution within the target and characterize its flux and energy spectrum entering a 40 μm diameter wire at the cone tip, and correlate these quantities with the amount of preformed plasma in the cone.

The experiment was performed on the Titan laser at LLNL, of $\lambda_0 = 1.054$ μm wavelength, 150 ± 10 J, focused to an 8 μm full width at half maximum (FWHM) focal spot in a 0.7 ± 0.2 ps pulse length. The intrinsic prepulse of the laser was measured at 8 ± 3 mJ in a 1.7 ns duration pulse prior to the main beam. Varying prepulse levels, up to 1 J, were produced by injecting an auxiliary nanosecond-duration laser colinear with the main short pulse laser. This auxiliary laser had a similar focal spot distribution as the main beam and was timed to overlap the intrinsic prepulse.

The target, shown in Fig. 1, was a 1 mm long Au hollow cone with 30° full opening angle, 20 μm wall thickness, 30 μm internal tip diameter, and 11 μm tip thickness. A 1.5 mm long, 40 μm diameter Cu wire was glued to the outer cone tip. The wire diameter is chosen to match the nominal 40 μm optimum ignition hot spot diameter in a FI target [7], and its quasi 1D geometry allows for single shot

0031-9007/12/108(11)/115004(5) 115004-1 © 2012 American Physical Society

PRL 110, 025001 (2013) PHYSICAL REVIEW LETTERS week ending 11 JANUARY 2013

Effect of Target Material on Fast-Electron Transport and Resistive Collimation

S. Chawla,[1,3] M. S. Wei,[2,*] R. Mishra,[1] K. U Akli,[2] C. D. Chen,[3] H. S. McLean,[3] A. Morace,[1,4] P. K. Patel,[3] H. Sawada,[1] Y. Sentoku,[5] R. B. Stephens,[2] and F.N. Beg[1]

[1]*Center for Energy Research, University of California, San Diego, La Jolla, California 92093, USA*
[2]*General Atomics, P.O. Box 85608, San Diego, California 92186, USA*
[3]*Lawrence Livermore National Laboratory, Livermore, California 94551, USA*
[4]*Department of Physics, University of Milano Bicocca, Milano 20126, Italy*
[5]*Department of Physics, University of Nevada, Reno, Nevada 89557, USA*
(Received 27 July 2012; published 7 January 2013)

The effect of target material on fast-electron transport is investigated using a high-intensity (0.7 ps, 10^{20} W/cm^2) laser pulse irradiated on multilayered solid Al targets with embedded transport (Au, Mo, Al) and tracer (Cu) layers, backed with millimeter-thick carbon foils to minimize refluxing. We consistently observed a more collimated electron beam (36% average reduction in fast-electron induced Cu $K\alpha$ spot size) using a high- or mid-Z (Au or Mo) layer compared to Al. All targets showed a similar electron flux level in the central spot of the beam. Two-dimensional collisional particle-in-cell simulations showed formation of strong self-generated resistive magnetic fields in targets with a high-Z transport layer that suppressed the fast-electron beam divergence; the consequent magnetic channels guided the fast electrons to a smaller spot, in good agreement with experiments. These findings indicate that fast-electron transport can be controlled by self-generated resistive magnetic fields and may have important implications to fast ignition.

DOI: 10.1103/PhysRevLett.110.025001 PACS numbers: 52.38.Dx, 52.38.Hb, 52.50.Jm, 52.65.Rr

Cone-guided fast-ignition (FI) inertial confinement fusion requires efficient energy transport of high-intensity short-pulse-laser-produced relativistic (or "fast") electrons through a solid cone tip to a high-density fuel core [1]. Specifically, successful ignition with a reasonable sized ignition laser requires high-conversion efficiency to 1–3 MeV electrons that have a minimum divergence [2,3]. Previous simulations show that fast-electron beam propagation in solid density plasmas are affected by a variety of mechanisms: scattering, resistive collimation [2,4], resistive filamentation [5], Ohmic heating, and electric field inhibition [6,7]. Evaluating the cone tip material, therefore, requires an understanding of the evolution of self-generated resistive fields and their cumulative effect on electron transport over the duration of the laser pulse. Previous material-dependent transport studies are limited; they have studied transport through only one material [8,9], simultaneously varied materials and fast-electron sources [10,11], or used energies much lower than presented here [11,12].

In this Letter, we report a systematic investigation of fast-electron transport in different materials (from high-Z Au to low-Z Al) without changing the electron source. We have demonstrated that a fast-electron beam can be collimated with a thin (~ 10 μm), high- or mid-Z transport layer buried a few μm beneath a low-Z Al layer without imposing a significant loss in forward-going electron energy flux. This is in contrast to previous 1D Fokker-Planck modeling predictions [13] that suggest high-Z Au material would increase divergence due to scattering and reduce the forward energy coupling, but it is consistent with the analytical model and 2D Fokker-Planck modeling showing stronger resistive collimation in high-Z plasmas by Bell and Kingham [4]. In addition, the collimation did not rely on complex structured targets [14] or a double laser pulse configuration [15], as shown in recent experimental work. $K\alpha$ fluorescence diagnostics, similar to those used in earlier work by Stephens *et al.* to measure fast-electron beam divergence [16], directly characterized fast-electron density distributions within the target. 2D collisional particle-in-cell (PIC) simulation results are in excellent agreement with experiments and show the formation, in high-Z transport targets, of strong resistive magnetic channels enveloped by a global B field that collimate initially divergent fast electrons. These magnetic channels extend into the subsequent lower resistance layers, maintaining the guidance of fast electrons.

The experiment used the Titan laser (1 μm wavelength, 150 J in 0.7 ps, 17 mJ average prepulse energy in 2.3 ns) at the Jupiter Laser Facility, Lawrence Livermore National Laboratory. An $f/3$ off-axis parabola focused the beam to a 10 μm (FWHM) spot with an incident angle of 17° onto the target front surface at $I_{\text{peak}} \sim 10^{20}$ W/cm^2. Figure 1 shows a schematic of the multilayered solid target, laser beam, and x-ray diagnostics. Targets had a common Al front layer (3 μm thick), a Z-transport layer [Au (8 μm), Mo (14 μm), or Al (33 μm)], and a Cu tracer layer (22 μm) buried 110 μm behind the Z-transport layer. The common front Al layer for all targets was to provide an identical fast-electron source for the transport study.

0031-9007/13/110(2)/025001(5) 025001-1 © 2013 American Physical Society

PRL 105, 015003 (2010) PHYSICAL REVIEW LETTERS week ending 2 JULY 2010

Relativistic Quasimonoenergetic Positron Jets from Intense Laser-Solid Interactions

Hui Chen,[1] S. C. Wilks,[1] D. D. Meyerhofer,[2,3] J. Bonlie,[1] C. D. Chen,[1] S. N. Chen,[1] C. Courtois,[4] L. Elberson,[1] G. Gregori,[5] W. Kruer,[1] O. Landoas,[4] J. Mithen,[5] J. Myatt,[2] C. D. Murphy,[5] P. Nilson,[2] D. Price,[1] M. Schneider,[1] R. Shepherd,[1] C. Stoeckl,[2] M. Tabak,[1] R. Tommasini,[1] and P. Beiersdorfer[1]

[1]*Lawrence Livermore National Laboratory, Livermore, California 94551, USA*
[2]*Laboratory for Laser Energetics, University of Rochester, Rochester, New York 14623, USA*
[3]*Department of Mechanical Engineering and Physics, University of Rochester, Rochester, New York 14623, USA*
[4]*CEA, DAM, DIF, F-91297 Arpajon, France*
[5]*Clarendon Laboratory, University of Oxford, OX1 3PU, United Kingdom*
(Received 15 January 2010; published 1 July 2010)

Detailed angle and energy resolved measurements of positrons ejected from the back of a gold target that was irradiated with an intense picosecond duration laser pulse reveal that the positrons are ejected in a collimated relativistic jet. The laser-positron energy conversion efficiency is $\sim 2 \times 10^{-4}$. The jets have ~ 20 degree angular divergence and the energy distributions are quasimonoenergetic with energy of 4 to 20 MeV and a beam temperature of ~ 1 MeV. The sheath electric field on the surface of the target is shown to determine the positron energy. The positron angular and energy distribution is controlled by varying the sheath field, through the laser conditions and target geometry.

DOI: 10.1103/PhysRevLett.105.015003 PACS numbers: 52.38.Ph, 52.59.−f

Relativistic positrons and positron jets are believed to exist in many astrophysical objects and are invoked to explain energetic phenomena related to gamma ray bursts and black holes [1–4]. On Earth, positrons from radioactive isotopes or accelerators are used extensively at low energies (sub-MeV) in areas related to surface science [5–8], positron emission tomography [9], basic antimatter science such as antihydrogen experiments [10,11], Bose-Einstein condensed positronium [12], and basic plasma physics [13]. Experimental platforms capable of producing the high-temperature positrons and high-flux positron jets [14] required to simulate astrophysical positron conditions have so far been absent. MeV temperature jets of positrons and electrons produced in these experiments provide a first step towards evaluating the physics models used to explain some of the most energetic phenomena in the Universe.

The pair producing mechanisms in intense laser-plasma interactions have been studied theoretically [15] and demonstrated experimentally in previous "proof-of-principle" experiments [16–18]. When intense lasers interact with solid targets a large number of fast electrons (>MeV) are created. These electrons create MeV bremsstrahlung photons in the target that, in turn, produce electron-positron pairs through the Bethe-Heitler process [15,19,20], unlike the direct laser pair production in vacuum which occurs via multiphoton absorption [21]. To date the angular distribution of the positrons ejected from the rear of the target and the source of the quasimonoenergetic nature of the observed positron energy distribution has been unknown. Here we present the first observations that the positrons are ejected in a well-defined cone from the back of the target, accelerated by several MeV due to the sheath field on the rear of the target. We demonstrate this by varying the transverse size of the target and the energy of the laser, both of which change the sheath field and influence the jet energies.

The electron-positron pair creation experiments reported here were performed using 1–10 picosecond laser pulses of 1.054 μm wavelength from the Titan laser [22] at the Lawrence Livermore National Laboratory and the OMEGA EP laser [23] at the University of Rochester's Laboratory for Laser Energetics. Laser energies from 100 to 850 J were focused into 8 (on Titan) to 50 (on OMEGA EP) micrometer diameter spots producing peak laser intensities from 1×10^{19} to 5×10^{20} W/cm^2. All targets were 1 mm thick solid gold with diameters between 1 and 20 mm. The experimental configuration is shown in Fig. 1. The positrons, electrons, and protons produced during the laser-target interaction were measured simultaneously using three absolutely calibrated electron-positron-proton spectrometers (EPPS) [24]. They were placed ~ 20 cm from the target at various angles to measure the energy spectrum of the electrons and positrons.

In the experiments, quasimonoenergetic, beamlike positron jets were observed. The positron energy spectra are shown in Fig. 2 for six shots with different laser and target conditions that controlled the positron peak energy. The energy of the peak (E_{peak}) of the positron distribution varied from 3 to 19 MeV, with an energy spread from 57% to 15%, equivalent to $E_{\text{peak}}/E_{\text{FWHM}} = 1.8$ to 6.9. The shot conditions are summarized in Table I.

The peak energy shift and the beamlike nature of the positron spectra arise due to sheath field effects from the rear of the target. The sheath field is established by the initial escaping electrons and the resulting electron cloud that forms around the target. It has been confirmed by proton or ion acceleration [25–27]. Since there are several orders of magnitude more electrons than positrons, the

0031-9007/10/105(1)/015003(4) 015003-1 © 2010 The American Physical Society

Physical and Life SCIENCES

Jupiter/Callisto

Callisto is the only operating high-intensity fs laser at LLNL. Was used for LPI and early FI work and has been used as a fast source for diagnostic development. Mainly it has been used for laser wakefield acceleration and now for developing a betatron. Too be closed FY2013.

PRL 103, 215006 (2009) PHYSICAL REVIEW LETTERS week ending 20 NOVEMBER 2009

Measurements of the Critical Power for Self-Injection of Electrons in a Laser Wakefield Accelerator

D. H. Froula,[1,*] C. E. Clayton,[2] T. Döppner,[1] K. A. Marsh,[2] C. P. J. Barty,[1] L. Divol,[1] R. A. Fonseca,[4] S. H. Glenzer,[1] C. Joshi,[2] W. Lu,[2] S. F. Martins,[4] P. Michel,[1] W. B. Mori,[2] J. P. Palastro,[1] B. B. Pollock,[1,3] A. Pak,[2] J. E. Ralph,[1,2] J. S. Ross,[1,3] C. W. Siders,[1] L. O. Silva,[4] and T. Wang[2]

[1]*L-399, Lawrence Livermore National Laboratory, P.O. Box 808, Livermore, California 94551, USA*
[2]*Department of Electrical Engineering, University of California, Los Angeles, California 90095, USA*
[3]*Department of Mechanical and Aerospace Engineering, University of California, San Diego, 9500 Gilman Drive, La Jolla, California 92093, USA*
[4]*GoLP/Instituto de Plasmas e Fusão Nuclear, Instituto Superior Técnico, Lisbon, Portugal*
(Received 17 June 2009; published 19 November 2009)

A laser wakefield acceleration study has been performed in the matched, self-guided, blowout regime producing 720 ± 50 MeV quasimonoenergetic electrons with a divergence $\Delta\theta_{\mathrm{FWHM}}$ of 2.85 ± 0.15 mrad using a 10 J, 60 fs 0.8 μm laser. While maintaining a nearly constant plasma density (3×10^{18} cm^{-3}), the energy gain increased from 75 to 720 MeV when the plasma length was increased from 3 to 8 mm. Absolute charge measurements indicate that self-injection of electrons occurs when the laser power P exceeds 3 times the critical power P_{cr} for relativistic self-focusing and saturates around 100 pC for $P/P_{cr} > 5$. The results are compared with both analytical scalings and full 3D particle-in-cell simulations.

DOI: 10.1103/PhysRevLett.103.215006 PACS numbers: 52.38.Kd, 41.75.Jv, 52.35.Mw

Thirty years ago, Tajima and Dawson predicted that an intense laser pulse can drive a plasma wake to produce 10–100 GeV/m electric fields which could accelerate electrons [1]. More than a decade later, laser-accelerator experiments used laser beat waves and the Raman forward instability to drive large amplitude plasma waves that generated electron beams with a continuous spectrum reaching high energies [2–6]. It was not until the laser technology advanced to having a sufficiently short pulse duration, at powers above 10 TW, that ~100 MeV quasi-monoenergetic electron beams accelerated by laser-produced wakefields were realized [7–9].

The ponderomotive force of the rising edge of an ultrashort ($\tau \sim 2\pi/\omega_p$) relativistically intense laser pulse propagating through an underdense plasma can completely blow out the electrons forming a spherical ion bubble around the pulse of the laser [10,11]. Here, ω_p is the plasma frequency. Electrons along the sheath of this bubble are pulled towards the laser axis and cross at the rear. Electrons residing within the region of high-accelerating and focusing fields can be self-injected into the accelerating structure if they gain enough velocity to catch up with the phase velocity of the wake driven by the laser. These self-injected electrons are then accelerated until they either outrun the slower moving accelerating potential of the wake over a "dephasing length" L_{dp} or the laser intensity is reduced so that no significant wake is excited. In order to maintain the intensity of the laser pulse over many Rayleigh lengths Z_r (typically $Z_r \ll L_{\mathrm{dp}}$), the diffraction of the laser field must be compensated by the refraction within the self-generated electron density channel of the wake [12–16] or an external waveguide [7].

The dephasing length (and therefore the electron energy) of a laser wakefield accelerator (LWFA) can be increased by reducing the electron plasma density since $L_{\mathrm{dp}}[\mathrm{cm}] \approx (\frac{P}{P_{cr}})^{1/6}(\frac{10^{18}\ \mathrm{cm}^{-3}}{n_e})^{4/3}$ [13]. However, for effective self-guiding and self-injection, the laser power must be maintained well above the critical power P_{cr} for self-focusing given by $P_{cr} = 17\omega_0^2/\omega_p^2$GW, where ω_0 is the laser frequency [13]. Simulations have suggested a power threshold for self-injection at low electron densities ($n_e \sim 10^{18}$ cm^{-3}) to be around $P/P_{cr} \approx 4$–8 [13,17], but this has not been experimentally demonstrated. Previous experiments in capillary discharge plasmas at low densities have shown thresholds for self-trapping [18] and ionization assisted self-trapping [19,20]. A study of the trapping threshold at high densities (low electron beam energies) was also performed in gas jets [5], but there have been no measurements of this threshold at $n_e < 5 \times 10^{18}$ cm^{-3} without an external guiding structure. At these low densities, laser pulses from high-power Ti:sapphire lasers with a typical pulse duration of about 50 fs are completely contained within the ion bubble and the electrons are accelerated to high energies.

In this Letter, we present the first GeV-class laser wakefield acceleration experiments where a self-injection threshold is demonstrated for densities below 5×10^{18} cm^{-3} in a gas jet without a guiding structure. For these densities, the laser power and spot size are such that a fully blown out self-guiding accelerating structure is excited over 8 mm of plasma and the laser pulse is contained within this bubble. The charge in the electron beams increases rapidly from 0.1 pC to a saturation level of ~100 pC when P/P_{cr} is increased from 3 to 5.

PRL 105, 105003 (2010) PHYSICAL REVIEW LETTERS week ending 3 SEPTEMBER 2010

Self-Guided Laser Wakefield Acceleration beyond 1 GeV Using Ionization-Induced Injection

C. E. Clayton,[1,*] J. E. Ralph,[2] F. Albert,[2] R. A. Fonseca,[3] S. H. Glenzer,[2] C. Joshi,[1] W. Lu,[1] K. A. Marsh,[1] S. F. Martins,[3] W. B. Mori,[1] A. Pak,[1] F. S. Tsung,[1] B. B. Pollock,[2,4] J. S. Ross,[2,4] L. O. Silva,[3] and D. H. Froula[2]

[1]*Department of Electrical Engineering, University of California, Los Angeles, California 90095, USA*
[2]*L-399, Lawrence Livermore National Laboratory, P.O. Box 808, Livermore, California 94551, USA*
[3]*GoLP/IPFN-IA, Instituto Superior Técnico, Lisboa, Portugal*
[4]*MAE Department, University of California, San Diego, La Jolla, California 92093, USA*
(Received 23 April 2010; published 1 September 2010)

The concepts of matched-beam, self-guided laser propagation and ionization-induced injection have been combined to accelerate electrons up to 1.45 GeV energy in a laser wakefield accelerator. From the spatial and spectral content of the laser light exiting the plasma, we infer that the 60 fs, 110 TW laser pulse is guided and excites a wake over the entire 1.3 cm length of the gas cell at densities below 1.5×10^{18} cm^{-3}. High-energy electrons are observed only when small (3%) amounts of CO_2 gas are added to the He gas. Computer simulations confirm that it is the K-shell electrons of oxygen that are ionized and injected into the wake and accelerated to beyond 1 GeV energy.

DOI: 10.1103/PhysRevLett.105.105003 PACS numbers: 52.38.Kd, 41.75.Jv, 52.35.Mw

Recent advances in high-power laser technology have led to major breakthroughs in the field of electron acceleration via the laser wakefield accelerator (LWFA) concept [1]. Among these is the experimental realization of the "bubble" or "blowout" regime [2–4], where an ultrashort but relativistically intense laser pulse ($c\tau \lesssim \lambda_p$ and $a_\ell \gtrsim 2$) propagating in an underdense plasma completely blows out all the plasma electrons. Here τ is the full width at half-maximum laser pulse duration, $a_\ell = \frac{eA}{mc^2}$ is the normalized vector potential of the focused laser pulse, and λ_p is the wavelength of the wakefield. These radially expelled plasma electrons are attracted back towards the laser axis by the space-charge force of the ions, forming a nearly spherical sheath around an "ion bubble" [3]. The electric field created by the resultant charge-density structure—the wakefield—has some distinct advantages: (i) an extremely large, radially uniform accelerating field that propagates at the group velocity of the laser pulse ($\approx c$), (ii) a longitudinally uniform but radially linear focusing field, and (iii) the ability to self-guide the laser pulse until it is depleted of its energy [3]. These characteristics provide for the generation of a high-quality, high-energy electron beam in a short distance, i.e., a "tabletop accelerator" [5].

Electrons injected into such an accelerator structure may gain energy until they outrun the wakefield over a dephasing length $L_{\mathrm{dp}}[\mathrm{cm}] \approx (P[\mathrm{TW}])^{1/3}(10^{18}\ \mathrm{cm}^{-3}/n_e)^{4/3}$ and gain a maximum energy $W_{\mathrm{max}}[\mathrm{GeV}] \approx 0.36(P[\mathrm{TW}])^{1/3} \times (L_{\mathrm{dp}}[\mathrm{cm}])^{1/2}$ [3]. Here, P is the peak laser power. Therefore, it is in principle possible to accelerate electrons to beyond a GeV energy in a distance of ~1 cm using a 100 TW-class laser provided that the electron density n_e is less than $\sim 1.5 \times 10^{18}$ cm^{-3}. The key issues for obtaining W_{max} are whether the wake can be maintained over L_{dp} and whether electrons can be injected and trapped into the wakefield at such a low density.

A number of recent experiments have addressed the issues of self-guiding [6,7], electron injection into the wake [8–12], and controlling the energy spread of the accelerated electrons [13–16]. However, the relatively high densities used in these experiments have limited their energy gain to less than 1 GeV. It should be noted that the only previous experiment to report a 1 GeV electron energy gain in a LWFA used a preformed plasma channel to guide the laser pulse [17]. However, using the self-guiding mechanism offered by the bubble regime can simplify a practical LWFA.

In this Letter, we show that the concepts of matched-beam, self-guided propagation and ionization-induced injection can be combined, at densities less than 1.5×10^{18} cm^{-3}, to accelerate electrons to beyond 1 GeV in a LWFA. In order to produce the requisite long and uniform volume of low-density gas (beyond the limits of currently used gas jets [14,16]), a new target platform was implemented: a 1.3-cm-long cell containing a gas mix of 97% He and 3% CO_2. The spatial and spectral content of the laser light exiting the plasma is measured and is consistent with self-guiding over the entire length of the gas cell (≈ 15 vacuum Rayleigh lengths) at a plasma density of 1.3×10^{18} cm^{-3}. Full, three-dimensional particle-in-cell (PIC) computer simulations using the code OSIRIS [18] show that it is indeed the K-shell oxygen electrons that are ionized and injected into the wake supported predominantly by the He electrons.

These experiments were performed at the Jupiter Laser Facility, Lawrence Livermore National Laboratory, using the 250 TW, 60 fsec Ti:sapphire Callisto laser system. Figure 1 shows the experimental setup where the laser beam was focused onto the front of the gas cell. The vacuum spot size w_0 was measured at low powers to be 15 μm at the $1/e^2$ intensity point. The fractional laser energy contained within the central laser spot was

PRL 107, 045001 (2011) PHYSICAL REVIEW LETTERS week ending 22 JULY 2011

Demonstration of a Narrow Energy Spread, ~0.5 GeV Electron Beam from a Two-Stage Laser Wakefield Accelerator

B. B. Pollock,[1,2,*] C. E. Clayton,[3] J. E. Ralph,[1] F. Albert,[1] A. Davidson,[3] L. Divol,[1] C. Filip,[1] S. H. Glenzer,[1] K. Herpoldt,[4] W. Lu,[3,5] K. A. Marsh,[3] J. Meinecke,[1] W. B. Mori,[3] A. Pak,[3] T. C. Rensink,[1] J. S. Ross,[1] J. Shaw,[3] G. R. Tynan,[2] C. Joshi,[3] and D. H. Froula[1,2]

[1]*Lawrence Livermore National Laboratory, 7000 East Avenue, Livermore, California 94550, USA*
[2]*University of California, San Diego, 9500 Gilman Drive, La Jolla, California 92093, USA*
[3]*University of California, Los Angeles, 405 Hilgard Avenue, Los Angeles, California 90095, USA*
[4]*University of Oxford, Wellington Square, Oxford, OX1 2JD, United Kingdom*
[5]*Department of Engineering Physics, Tsinghua University, Beijing, China, 100084*
(Received 13 April 2011; published 18 July 2011)

Laser wakefield acceleration of electrons holds great promise for producing ultracompact stages of GeV scale, high-quality electron beams for applications such as x-ray free electron lasers and high-energy colliders. Ultrahigh intensity laser pulses can be self-guided by relativistic plasma waves (the wake) over tens of vacuum diffraction lengths, to give >1 GeV energy in centimeter-scale low density plasmas using ionization-induced injection to inject charge into the wake even at low densities. By restricting electron injection to a distinct short region, the injector stage, energetic electron beams (of the order of 100 MeV) with a relatively large energy spread are generated. Some of these electrons are then further accelerated by a second, longer accelerator stage, which increases their energy to ~0.5 GeV while reducing the relative energy spread to <5% FWHM.

DOI: 10.1103/PhysRevLett.107.045001 PACS numbers: 52.38.Kd, 41.75.Jv, 52.35.Mw

State-of-the-art conventional radio-frequency linear accelerators currently produce electron beams with up to 50 GeV energies by staging many 100 MeV sections [1]. Future proposed x-ray free electron lasers (such as the European XFEL) will produce 20 GeV electron beams which, when passed through an undulator, will provide extremely bright x-ray sources. Facilities of this scale require substantial lengths (several kilometers) to achieve high electron energies due to limits on the maximum accelerating gradient imposed by cavity damage threshold considerations (< 100 MeV/m). Alternatively, laser wakefield accelerators (LWFAs) can support gradients exceeding 100 GeV/m [2,3], opening the possibility of dramatically reducing the required length to produce high-energy beams. Current laser technology limits the length of these devices to a few centimeters and, therefore, the energy gain to a few GeV. Coupling of multiple independent high-energy gain LWFA stages could provide a path forward for achieving future compact, high-energy particle sources.

Recent experiments have demonstrated self-guiding [4] of ultrashort laser pulses in the blowout regime of a LWFA, where extremely nonlinear wakefields are produced in underdense plasmas [5–12]. In this regime the rising edge of an intense, short laser pulse tunnel ionizes low-Z gas, and the ponderomotive force of the laser expels electrons radially outward to a maximum distance $R \approx 2\sqrt{a_0}c/\omega_p$ [13], determined by balancing the transverse ponderomotive force with the restoring space charge force of the stationary ions. Here $a_0 = eA/mc$ is the normalized vector potential of the laser, and $\omega_p = \sqrt{n_e e^2/\epsilon_0 m_e}$ is the electron plasma frequency. The blown-out region at the front of the pulse acts as a channel to guide the majority of the laser light, while behind the laser pulse electrons are pulled back toward the axis. This produces an electron plasma wave (the wake) with a phase velocity v_ϕ nearly equal to the group velocity v_g of the laser.

When the laser pulse length approaches $c\tau \approx R$, a nearly spherically shaped wake is formed, within which nearly all of the electrons are blown out. The trajectories of these electrons form a sheath around the ions [14], and the longitudinal electric field structure near the axis of the wake is ideal for accelerating a high-quality electron beam [15]. Electrons injected into the wake (via self-injection [16], ionization-induced injection [17–19], colliding pulses [20], etc.) become trapped in the wake potential if they gain a longitudinal velocity $v = v_\phi$ and continue accelerating in the longitudinal electric field of the wake (of the order of 100 GeV/m for electron densities of ~10^{18} cm^{-3} [13]). Over a dephasing length $L_{\mathrm{deph}} \approx (2/3)(\omega_{\mathrm{wave}}^2/\omega_p^2)R$, these electrons, traveling at nearly c, move forward in the wake to its midplane, where the sign of the electric field reverses and electrons decelerate. The dephasing limited energy gain is given by $W_{\mathrm{max}} = E_z L_{\mathrm{deph}} = 0.37(P[\mathrm{TW}])^{1/3}(n_e/18^{18}\ \mathrm{cm}^{-3})^{-2/3}$, where E_z is the dephasing length averaged electric field within the wake [13]. Therefore, for powers less than 80 TW, electron densities below 2×10^{18} cm^{-3} are required to achieve electron energy gains above 1 GeV in this regime.

Physical and Life SCIENCES

Jupiter/COMET

COMET is a versatile system (several beam paths, ps and ns beams) with a 3-5-minuted rep rate. Used mainly for spectroscopy, technique development, Calibration and testing of NIF diagnostics.

First observation of the optimal plasma scale length for THz radiation from interactions of relativistic sub-picosecond laser pulses with solid targets

G. Q. Liao[1], L. N. Su[1], Y. Zheng[1], M. Liu[1], W. C. Yan[1], C. Li[1], Y. T. Li[1], J. Dunn[2], J. Nilsen[2], W. M. Wang[1], Z. M. Sheng[1,3], L. M. Chen[1], J. L. Ma[1], X. Lu[1], J. Zhang[1,3*]

[1] Beijing National Laboratory for Condensed Matter Physics, Institute of Physics, Chinese Academy of Sciences, Beijing 100190, China

[2] Lawrence Livermore National Laboratory, 7000 East Avenue, Livermore, CA 94551, USA

[3] Key Laboratory for Laser Plasmas (MoE) and Department of Physics, Shanghai Jiao Tong University, Shanghai 200240, China

Terahertz (THz) radiation from interactions of 0.5-ps relativistic laser pulses with solid targets is studied when a large-scale underdense preplasma is presented before the main pulse on the COMET laser system at Lawrence Livermore National Laboratory. The angular distribution, polarization and spectrum of THz radiation are characterized. It is found that THz radiation in the specular direction (+62.5°) strongly depends on the preplasma scale length. It is the first experimental observation of the existence of an optimal plasma density scale length for powerful THz radiation. Within an appropriate range of the plasma scale length, the THz radiation observed is attributed to the linear mode conversion mechanism probably. By optimizing the plasma scale length, strong THz radiation with energies up to ~ millijoules (mJ) and the energy conversion efficiency up to 10^{-4} can be generated. Such strong THz radiation will allow for many applications such as nonlinear THz sciences.

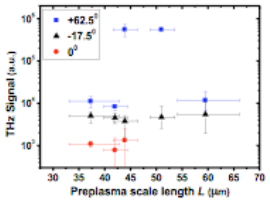

Fig.1. THz intensity as a function of the preplasma scale length.

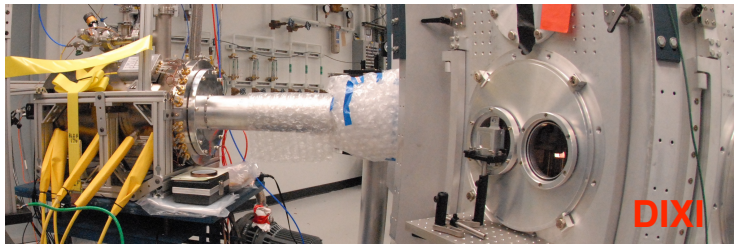

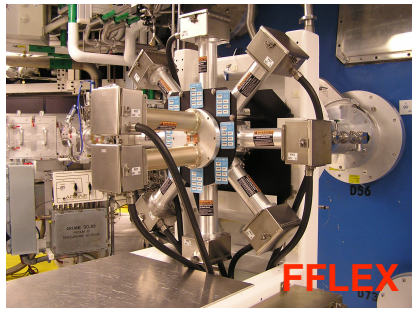

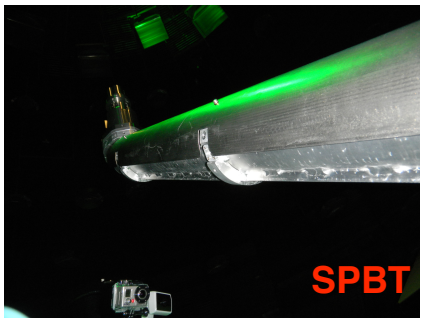

Jupiter/Europa

Ti:Sapph Europa was used for development of FDI and fs WDM studies on thin targets. Europa has been cannibalized for parts but is a good university-class fs laser.

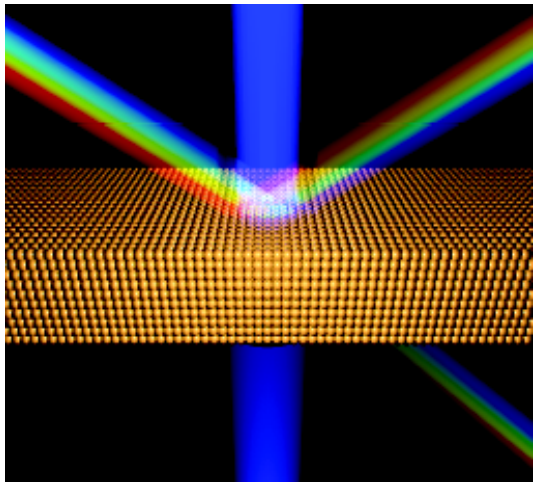

- Warm Dense Matter is created by isochoric laser heating of free-standing nanofoils, leading to a non-equilibrium state with $T_e >> T_i$.

PRL 96, 255003 (2006) PHYSICAL REVIEW LETTERS week ending 30 JUNE 2006

Broadband Dielectric Function of Nonequilibrium Warm Dense Gold

Y. Ping,[1] D. Hanson,[2] I. Koslow,[2] T. Ogitsu,[1] D. Prendergast,[1] E. Schwegler,[1] G. Collins,[1] and A. Ng[1,2]
[1]*Lawrence Livermore National Laboratory, Livermore, California, USA*
[2]*Department of Physics & Astronomy, University of British Columbia, Vancouver, British Columbia, Canada*
(Received 15 May 2006; published 26 June 2006)

We report on the first single-state measurement of the broadband (450–800 nm) dielectric function of gold isochorically heated by a femtosecond laser pulse to energy densities of $10^6 - 10^7$ J/kg. A Drude and an interband component are clearly seen in the imaginary part of the dielectric function. The Drude component increases with energy density while the interband component shows both enhancement and redshift. This is in strong disagreement with predictions of a recent calculation of dielectric function based on limited Brillouin zone sampling.